environments

MDPI

Article

From Invasion to Valorization: Adsorbent Applications of *Acacia dealbata* Biomass in Portugal

Morgana Macena [1,2,*], Bruno Esteves [2], Jackelline S. Pinto [3], Rui Novais [4], Ana P. F. Caetano [4], Lucas Grosche [5], Helena Pereira [1] and Luísa Cruz-Lopes [2]

1 CEF-Forest Research Centre, Associate Laboratory TERRA, School of Agriculture, University of Lisbon, 1349-017 Lisboa, Portugal; hpereira@isa.ulisboa.pt
2 CERNAS-IPV Research Centre, Polytechnic University of Viseu, Campus Politécnico, Repeses, 3504-510 Viseu, Portugal; bruno@estgv.ipv.pt (B.E.); lvalente@estgv.ipv.pt (L.C.-L.)
3 ESTGV-IPV, Escola Superior de Tecnologia e Gestão de Viseu, Campus Politécnico, Repeses, 3504-510 Viseu, Portugal; pv31795@alunos.estgv.ipv.pt
4 Department of Materials and Ceramic Engineering, CICECO-Aveiro Institute of Materials, University of Aveiro, Campus Universitário de Santiago, 3810-193 Aveiro, Portugal; ruimnovais@ua.pt (R.N.); anacaetano@ua.pt (A.P.F.C.)
5 4iTec Lusitânia S.A., Lugar do Pombal, Zona Industrial do Salgueiro, 3530-259 Mangualde, Portugal; lucas.grosche@4iteclusitania.pt
* Correspondence: morgana@estgv.ipv.pt

Abstract

Acacia dealbata, an invasive species in Portugal, produces large amounts of residual biomass during control operations, thereby presenting challenges and opportunities for sustainable valorization. Heavy metal contamination, including zinc (Zn), remains a critical environmental challenge due to its widespread industrial release and potential ecotoxicological impacts. This study explores the potential use of *A. dealbata* biomass as a biosorbent for zinc removal from aqueous solutions, comparing the performance of natural biomass and *A. dealbata* charcoal fines. Adsorption isotherms, kinetics, and surface characterizations were conducted to evaluate their physicochemical properties and sorption efficiency. The *A. dealbata* charcoal fines exhibited a significantly higher specific surface area (33 $m^2\ g^{-1}$) and total pore volume (0.030 $cm^3\ g^{-1}$) compared with the untreated biomass (1.4 $m^2\ g^{-1}$ and 0.004 $cm^3\ g^{-1}$, respectively). Despite these structural differences, both materials demonstrated similar maximum adsorption capacities (23.36 and 23.79 mg g^{-1} for natural and charcoal fines, respectively). These results indicate that untreated *A. dealbata* biomass can perform as a biosorbent comparably to its carbonized form, representing a simple, low-cost, and sustainable alternative for heavy metal removal, offering a low-energy and sustainable alternative for Zn remediation.

Keywords: *Acacia dealbata*; invasive species; biomass valorization; biosorption capacity; zinc removal; wastewaters

Academic Editors: Gabriel Gascó Guerrero, Ana Méndez and Jorge Paz-Ferreiro

Received: 15 November 2025
Revised: 30 December 2025
Accepted: 3 January 2026
Published: 1 February 2026

1. Introduction

There are approximately 1380 species of Acacia distributed globally, with natural occurrences primarily in Australia (around 1000 species), Africa (144 species), Asia (89 species), and the Americas (a total of 185 species). At least eight Australian acacia species have been introduced into Southern Europe, where they are classified as invasive [1]. *Acacia dealbata* Link, in particular, is considered invasive across Europe, America

and Africa, with proven impacts on soil properties and native plant communities, thereby threatening local biodiversity [2].

The intentional introduction of non-native species has historically been motivated by various objectives, including commercial, ornamental, or ecological restoration purpose [3]. *A. dealbata* was introduced in Southern Europe in the 19th century as an ornamental plant [1,4,5], and now is widely established in France, Italy, Portugal, and Spain [1].

This species has a pronounced invasive potential in Portugal, which is largely explained by its prolific seed production, high germination rate (>70%), rapid growth, and allelopathic capacity [4,6]. According to the most recent National Forest Inventory, the area invaded by acacias expanded between 1995 and 2010, from 2701 ha to 5351 ha [7], while field observations allow estimating a much higher area coverage nowadays. This increase poses a considerable ecological threat to Portuguese ecosystems [5].

Wildfires and climate change constitute major drivers of environmental disruption and facilitate the spread of alien species by altering forest structure and function [8,9]. Portugal is the European country most impacted by wildfires [10], which exacerbates the issue of biological invasions, as alien species frequently display greater adaptive capacity to new edaphoclimatic conditions than native flora [3].

Several acacia species are pyrophytic, with fire acting as a stimulus for germination and dispersal, while gaining a competitive advantage over native vegetation under increasingly hot and dry climatic regimes [4,5]. Evidence indicates that acacias not only demonstrate resilience to high-severity wildfires but also contribute to increased fuel accumulation in the short and medium term [11]. In addition, many acacia species persist in viable soil seedbanks [11,12], which can promote large-scale germination events following fire disturbances [9,11,13]. For example, a widespread invasion of *A. longifolia* was documented in Portugal subsequent to a wildfire event [14].

Acacia invasions threaten biodiversity conservation within protected areas, disrupt ecosystem services, and negatively impact the forest sector. In response, control strategies aimed at mitigating their proliferation have been implemented [15]. However, invasive plant control is typically costly and demands continuous financial investment [16]. Moreover, these interventions generate substantial amounts of residual biomass, which is commonly incinerated for energy recovery or deposited in landfills [16,17]. For instance, the control operation of just 2 ha of *A. dealbata* generated approximately 140 tons of biomass [3].

Exploring high-value applications for acacias biomass could help to offset these costs, thereby improving the economic sustainability of management practices. Several studies have investigated the valorization of several Acacia species for its chemical or pharmaceutical potential [13,18,19], cellulose or pulp production [20–22], adsorbents application [23–25], and as a renewable energy source, such as bioethanol or pellets [17,26,27]. However, the valorization of *A. dealbata* is still scarcely explored. Therefore, the management of acacias, particularly of *A. dealbata*, is of critical importance, and their valorization as bio-adsorbents represents a promising approach.

Heavy metals are persistent environmental pollutants capable of accumulating throughout the food chain, and due to their high solubility and mobility, they pose serious risks to both ecosystems and human health. Although zinc is considered one of the less toxic heavy metals and intoxication cases are relatively rare, excessive exposure can still cause adverse effects such as loss of appetite, nausea, irritability, and muscle stiffness [28,29]. Heavy metal contamination, including zinc (Zn), is a growing concern due to intensive industrial discharge. Zn commonly enters water bodies through galvanization, electroplating, mining, fertilizers, pigments, and wastewaters from the textile and leather sectors. Industrial effluents may contain Zn concentrations exceeding 50–200 mg L^{-1}, far

above permissible discharge limits. These levels justify the need for effective, low-cost water remediation technologies.

In this context, the removal of heavy metals from aqueous systems has become a crucial environmental challenge. Among the available treatment methods, adsorption stands out as one of the most efficient, rapid, and cost-effective techniques for metal removal [30,31]. This process offers high versatility and operational simplicity, making it particularly suitable for large-scale applications. Nevertheless, improving adsorbent performance often requires chemical or thermal modification, which can increase energy consumption and chemical use, potentially limiting its sustainability [30].

In this work, we reinforce the environmental relevance of Zn removal and provide a scientifically grounded justification for studying its mitigation using low-cost materials. We also highlight the novelty of evaluating Portuguese *A. dealbata* biomass and directly comparing untreated biomass with commercially produced charcoal fines, a comparison not previously reported. Charcoal fines derived from *A. dealbata* biomass, and untreated acacia biomass were prepared, characterized, and evaluated as bio-adsorbents for Zn(II) removal from aqueous solutions, with adsorption behavior analyzed through isotherm and kinetic models.

2. Materials and Methods

2.1. Sample Preparation

The biomass of *Acacia dealbata* was collected in the Viseu region, Portugal, by harvesting young trees. The stem and branches, including the wood and bark components, were kept while foliage was discarded. The material, without pre-treatment, herein coded as AN, was milled (Fritsch pulverisette 19, Idar-Oberstein, Germany) and sieved (Retsch AS200; Retsch-Allee, Haan, Germany) to obtain fractions of different particle sizes; the powder fraction (~177 µm) was selected for use as a bio-adsorbent (untreated acacia biomass).

The *Acacia dealbata* charcoal fines (AB) were produced by Kool Nature (São Paio de Mondego, Portugal) from dust and fines separated from vegetal charcoal derived from *A. dealbata* prior to use. This charcoal, marketed as BioCarvão or Ekoology, was obtained through slow pyrolysis at 800 °C for 8–12 h under strictly controlled low-oxygen conditions, maintaining O_2 ingress below 2% to ensure efficient carbonization and minimal volatile release. The resulting material contains >94% fixed carbon, <3% volatile matter, and negligible moisture. The charcoal fines were sieved to the same granulometric range as AN to ensure comparability.

2.2. Sample Characterization

High-resolution scanning electron microscopy (SEM) was conducted with a Hitachi SU-70 microscope (Hitachi High-Tech Corp., Tokyo, Japan) operated at 15 kV and equipped with energy-dispersive X-ray spectroscopy (EDS, Brüker, Germany) for elemental analysis. Samples were mounted on aluminum stubs and coated with a conductive carbon film using an Emitech K950X evaporator (Emitech Group, Montignyle-Bretonneux, France).

Powder X-ray diffraction (XRD) patterns were obtained at room temperature on a θ/θ diffractometer Empyrean PANalytical diffractometer (Malvern Panalytical B.V., Almelo, The Netherlands) equipped with a PIXcel 1D detector and Cu Kα radiation (λ_1 = 1.5406 Å, λ_2 = 1.5444 Å) at 45 kV and 40 mA, using Bragg–Brentano geometry and continuous scanning from 5° to 80° (2θ) with a 0.01° step size.

The specific surface area and porous properties of AN and AB powders were measured via N_2 adsorption–desorption isotherms using the Brunauer–Emmett–Teller (BET) and BJH methods, respectively, on a Gemini V-2380 analyzer (Micromeritics Instrument Corporation, Norcross, GA, USA).

2.3. Adsorption Tests

All adsorption experiments were conducted in triplicate under identical conditions at room temperature, using an adsorbent dosage of 4 g L^{-1}. Following adsorption, filtration was performed by gravity using standard paper filters, ensuring accurate AAS quantification and preventing particle interference. The influence of pH was assessed by measuring the adsorption efficiency across a pH range of 3 to 9. Control tests without adsorbent were conducted to quantify Zn precipitation as $Zn(OH)_2$ at pH values > 7. All subsequent experiments were carried out at the pH value that yielded the highest removal efficiency.

Adsorption isotherms were evaluated by conducting experiments with Zn(II) ion concentrations ranging from 10 to 50 mg L^{-1}, and the resulting data were fitted to the Langmuir and Freundlich models, respectively, Equations (1) and (2).

$$\frac{1}{q_e} = \frac{1}{q_{max}} + \left(\frac{1}{K_L \times q_{max}}\right) \times \frac{1}{C_e} \quad (1)$$

$$\ln q_e = \ln K_F + \frac{1}{n} \times \ln C_e \quad (2)$$

where q_e (mg g^{-1}) represents the quantity of ions adsorbed in each g of adsorbent material, qmax corresponds to the saturation capacity of the adsorbent material, C_e (mg L^{-1}) is the equilibrium concentration, and K_L is the Langmuir constant. The n of Freundlich indicates the magnitude of the surface heterogeneity, and the K_F is the Freundlich constat.

Additionally, the R_L of Langmuir was calculated to describe the favorability of the adsorption, according to Equation (3).

$$R_L = \frac{1}{1 + C_0 \times K_L} \quad (3)$$

where C_0 is the initial concentration of the adsorbate. The value of R_L indicates the nature of the adsorption process: $R_L < 1$ means favorable, $R_L = 1$ is linear, $R_L > 1$ is unfavorable, and $R_L = 0$ indicates irreversible adsorption.

2.4. Kinetic Studies

Kinetic experiments were performed at an initial Zn(II) concentration of 20 mg L^{-1} over contact times between 1 and 120 min, and the adsorption dynamics were analyzed using the pseudo-first-order (PFO) model presented by Equation (4).

$$\ln(q_e - q_t) = \ln(q_e) - k_1 \times t \quad (4)$$

where q_e and q_t (mg g^{-1}) represents the amount of solute absorbed at equilibrium and the adsorbed at time t, respectively; k_1 (min) is the pseudo-first-order rate constant, representing the rate at which adsorption sites are occupied. Higher k_1 values indicate a faster adsorption process.

Adsorption is interpreted as the interaction between the adsorbate and two independent active sites on the adsorbent, as described by the pseudo-second-order kinetic model. The linearized form of this model is presented in Equation (5).

$$\frac{t}{q_t} = \frac{1}{k_2 q_e^2} + \frac{t}{q_e} \quad (5)$$

In this model, k_2 (g $mmol^{-1}$ min^{-1}) denotes the pseudo-second-order adsorption rate constant. Based on k_2, the initial adsorption rate h (mg g^{-1} min^{-1}) is defined as shown in Equation (6).

$$h = k_2 \times q_e^2 \quad (6)$$

The Weber–Morris intraparticle diffusion model [32] was applied to gain deeper insight into the rate-limiting steps governing Zn(II) adsorption onto the AN and AB biosorbents. The model is expressed by Equation (7).

$$q_t = k_{id} \times t^{1/2} + C \quad (7)$$

where k_{id} (mg g^{-1} $min^{-1/2}$) is the intraparticle diffusion rate constant, and C (mg g^{-1}) is the intercept associated with boundary-layer resistance.

The residual Zn(II) concentration in solution was quantified by atomic absorption spectroscopy (AAS) and calculated using Equation (8).

$$\%\text{adsorption} = \frac{C_i - C_f}{C_i} \times 100 \quad (8)$$

C_i is the initial concentration of the metal in the solution (mg L^{-1}) and C_f is the concentration of the metal remaining in the solution (mg L^{-1}) after the adsorption process, measured by AAS.

3. Results

3.1. Characterization of the Natural and Modified Acacia Biomass

The SEM micrographs and EDS spectra of the AN and AB samples are shown in Figures 1 and 2, respectively. Natural acacia (AN) contains small granular particles with cellular fragments that contain various cellular structures: small and rather isodiametric cells, which are typical of wood rays, shown in fragment 1, while a considerable amount of long cells representing the main wood fiber and vessel structures are presented in fragment 2.

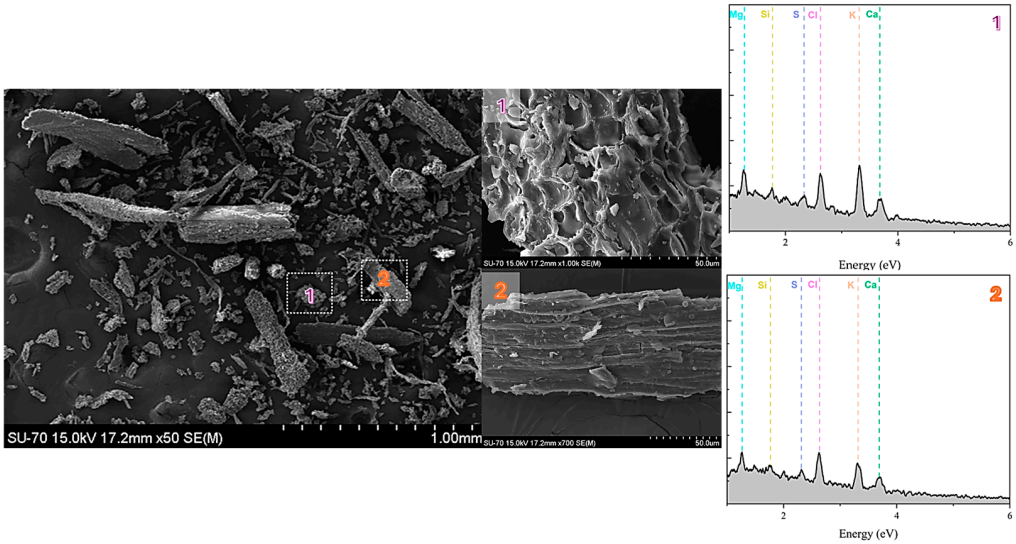

Figure 1. SEM micrographs of the *Acacia dealbata* untreated sample (AN) and EDS spectra recorded from two particulate fragments (1–2).

Figure 2 reveals that the acacia charcoal fines have a heterogeneous structure combining numerous small fragments mostly with approximate spherical shape with longer fragments more of a fibrous nature. For instance, fragment 2 shows a vessel structure with vessel elements measuring about 10 µm in width and 40 µm in length.

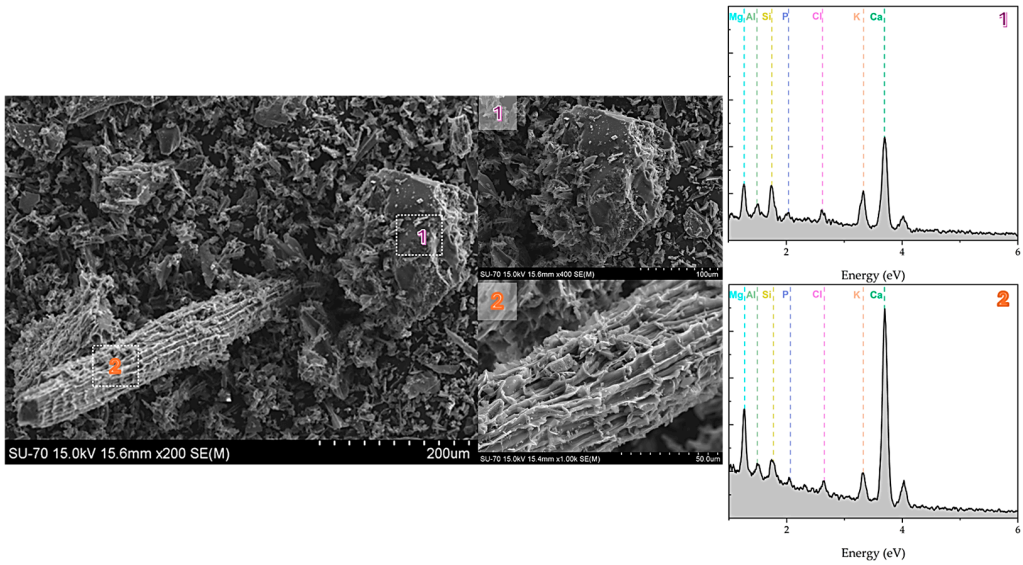

Figure 2. SEM micrographs of the *Acacia dealbata* charcoal fines (AB) and EDS spectra recorded from two particulate fragments (1–2).

The XRD pattern (Figure 3) of the AN shows that the material is predominantly amorphous, containing minor crystalline features. In contrast, the charcoal fines (AB) exhibit distinct diffraction peaks corresponding to calcite ($CaCO_3$), suggesting that mineral transformations occurred during the pyrolysis process.

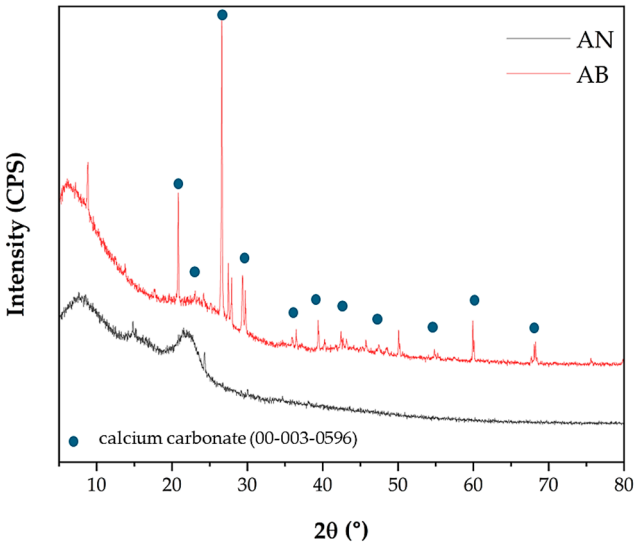

Figure 3. XRD patterns of the *Acacia dealbata* untreated biomass (AN) and charcoal fines (AB).

To provide additional insights into the biosorbents' physical properties, the specific surface area was determined by the multipoint BET method. The specific surface area (SSA) of AN was 1.4 m^2g^{-1} and total pore volume of 0.004 cm^3g^{-1}, whereas AB shows much higher SSA (33 m^2g^{-1}) and total pore volume (0.030 cm^3g^{-1}).

The N_2 adsorption–desorption isotherms and pore size distribution curves are presented in Figure 4a and 4c, respectively. The pore size distribution of the AN (Figure 4b) and AB (Figure 4d) were estimated using the Barret-Joyner-Halenda (BJH) method.

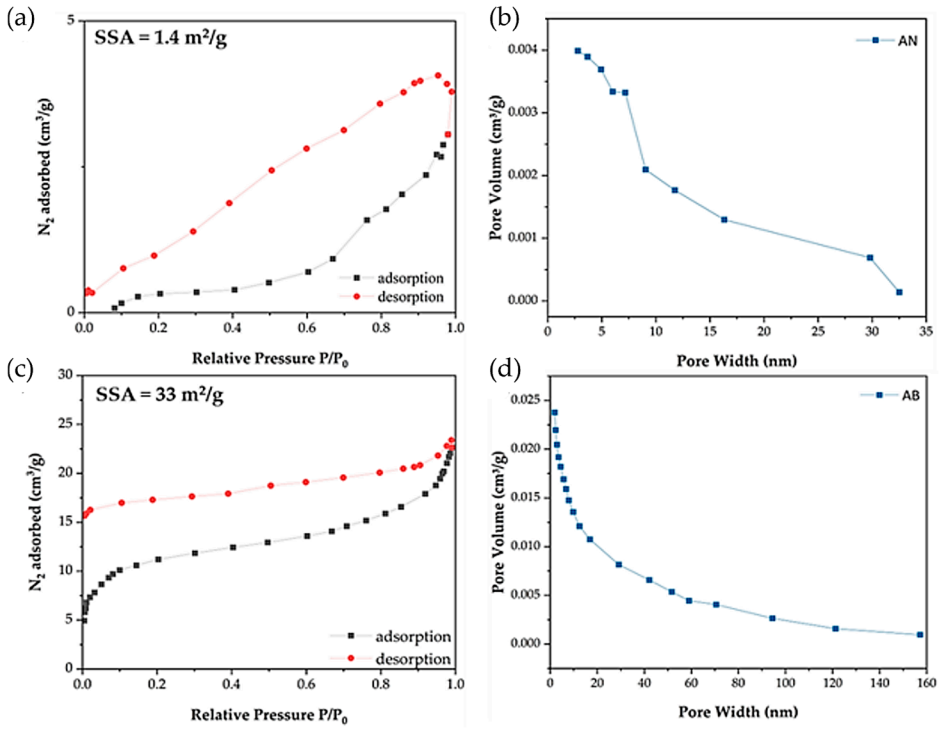

Figure 4. N_2 adsorption–desorption isotherms (**a**,**c**) and pore size distribution curves (**b**,**d**) of *Acacia dealbata:* (**a**,**b**) correspond to the untreated (AN) sample; (**c**,**d**) correspond to the charcoal fines (AB).

The AN has a smaller pore volume (0–0.004 cm^3g^{-1}) and a narrower pore width (2–33 nm) compared with AB (0–0.025 cm^3g^{-1} and 2–157 nm, respectively). AN powder presents a type H_2 hysteresis loop, which is typical for complex pore structures with the presence of a very steep desorption branch, which can probably be attributed to pore blocking [33]. On the other hand, the AB powder presents a more similar hysteresis loop of type H_3, where the adsorption branch resembles a type II isotherm, characteristic of macropores and aggregates of plate-like particles [34].

Based on the physicochemical characterization of the adsorbent materials (AN and AB), the potential mechanisms involved in the adsorption of Zn(II) ions onto the active sites on the biomass surface are summarized in Figure 5.

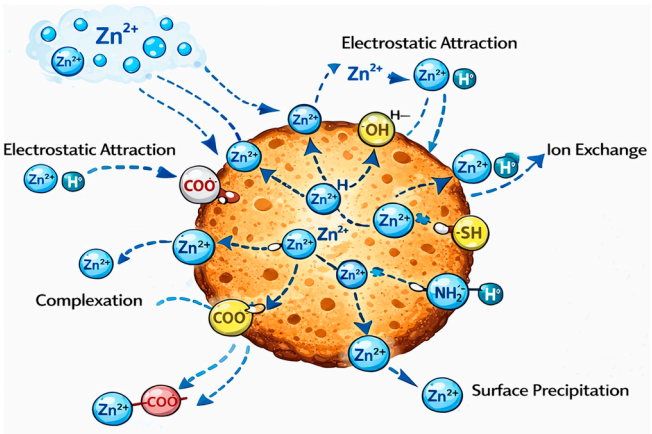

Figure 5. Proposed mechanisms for Zn(II) adsorption on natural acacia (AN) and charcoal fines (AB), including electrostatic interactions, ion exchange, and surface complexation at active functional groups—hydroxyl (-OH), carboxyl (-COO), carbonyl (-C=O), amine ($-NH_2$), etc.

3.2. Experimental Adsorption Tests, Isotherm and Kinetics

The pH plays a crucial role in the adsorption process, as it governs both the surface charge of the adsorbent and the degree of ionization of the adsorbate, thereby directly affecting the adsorption efficiency and mechanism. The best pH for zinc removal by both acacia-based biosorbents was investigated (Figure 6).

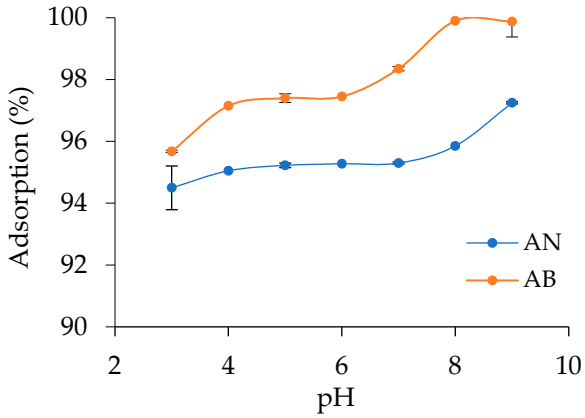

Figure 6. Study of the pH effect on the adsorption of Zn ions by the *Acacia dealbata* biosorbents (natural—AN and charcoal fines—AB).

The adsorption rate increased with rising solution pH. However, at pH values above 8 or below 4, zinc ions are susceptible to precipitation, mostly as zinc hydroxide ($Zn(OH)_2$), which may interfere with the adsorption measurements. Therefore, a near-neutral pH was considered as the optimal condition for zinc ion removal by both acacia-based biosorbent materials, achieving removal efficiencies of approximately 98% for acacia charcoal fines (AB) and 95% for natural acacia (AN). These results indicate that an acid to neutral medium minimizes H^+ competition for active sites while preventing the formation of $Zn(OH)_2$, thus optimizing ion–surface interactions.

The results of the adsorption modeling based on the Langmuir and Freundlich isotherm models are presented in Figure 7, and the corresponding model parameters are summarized in Table 1.

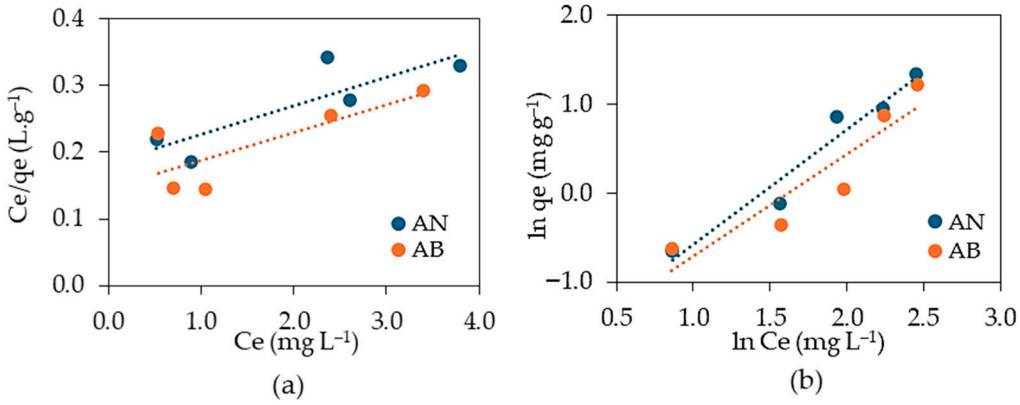

Figure 7. Plotting of Langmuir (**a**) and Freundlich (**b**) isotherm models for the adsorption of Zn ions onto *Acacia dealbata* biosorbents (natural (AN) and charcoal fines (AB).

Table 1. Parameters of Langmuir and Freundlich isotherm models for the adsorption of Zn ions onto *Acacia dealbata* biosorbents: natural (AN) and charcoal fines (AB).

Model Parameter	Biosorbent Type	
	AN	**AB**
Langmuir		
qmax (mg g^{-1})	23.36	23.79
K_L (L mg^{-1})	0.23	0.29
R^2	0.71	0.62
R_L	0.30	0.26
Freundlich		
n	1.29	1.15
$1/n$	0.77	0.87
K_F (mg g^{-1}).(L $mg^{-1})^{1/n}$	0.16	0.16
R^2	0.95	0.85

The isothermal adsorption pattern was comparable for both adsorbent materials. The experimental data fitted the Freundlich model, which describes multilayer adsorption, with correlation coefficients of 0.95 and 0.85 for the natural acacia (AN) and acacia charcoal fines (AB), respectively. The maximum adsorption capacity (qmax), estimated using the Langmuir model, was also very similar for both materials, with values of 23.36 and 23.79 mg g^{-1} for AN and AB, respectively.

Adsorption is generally considered favorable when the Freundlich constant, n, lies between 1 and 10; higher n values indicate stronger interactions between the adsorbate and the adsorbent. Since the Freundlich constant n values, 1.29 (AN) and 1.15 (AB), were close to 1, the adsorption can be described as nearly linear. Moreover, the Langmuir factor $R_L < 1$ confirms that the adsorption process was favorable under the conditions studied.

Regarding the reaction kinetics, the time-dependent adsorption behavior is illustrated in Figure 8. The parameters of the pseudo-first-order (PFO) and pseudo-second-order (PSO) kinetic models, calculated based on the experimental data, are presented in Table 2.

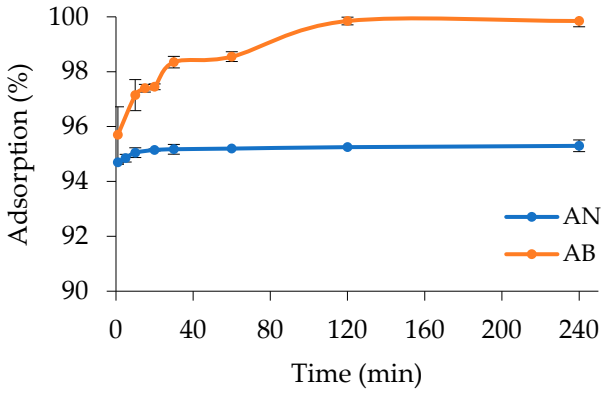

Figure 8. Adsorption of Zn ions by *Acacia dealbata* biosorbents (AN and AB) over time.

The time-dependent adsorption study revealed distinct behaviors between the two adsorbent materials. In both cases, adsorption occurred rapidly, with more than 90% of zinc ions being removed within the first few minutes of contact. However, the charcoal fines exhibited a slightly more variable adsorption profile, showing a gradual increase over time, whereas the natural acacia displayed a steadier trend, suggesting faster saturation of its available surface active-sites. This behavior indicates that, despite structural differences between the materials, both possess high initial affinity for Zn, with equilibrium being reached within a short contact time.

Table 2. Kinetic parameters of the pseudo-first-order (PFO) and pseudo-second-order (PSO) models applied to the adsorption onto *Acacia dealbata* biosorbents (AN and AB).

Model Parameter	Biosorbent Type	
	AN	**AB**
PFO		
k_1 (L min^{-1})	7.88×10^{-3}	1.42×10^{-2}
q_e calc (mg g^{-1})	0.57	1.00
q_e exp (mg g^{-1})	76.14	79.88
R^2	0.78	0.95
PSO		
k_2 (g mg^{-1}.min)	3.85×10^{-1}	4.16×10^{-2}
h (mg g^{-1}.min)	2240.65	266.54
q_e calc (mg g^{-1})	76.24	80.00
q_e exp (mg g^{-1})	76.14	79.88
R^2	1.00	1.00

According to the kinetic model fitting, the adsorption process followed the pseudo-second-order (PSO) model in both cases, with correlation coefficients (R^2) of 1.00 for the natural acacia and acacia charcoal fines. These results suggest that the adsorption mechanism is predominantly governed by chemisorption.

Given the chemisorption-driven kinetics suggested by the PSO model, it was essential to evaluate the contribution of mass-transfer mechanisms to the overall adsorption process. The intraparticle diffusion plots presented in Figure 9 illustrate the Weber–Morris profiles for Zn adsorption onto natural (AN) and charcoal fines (AB) of acacia, revealing a clear multilinear behavior for both biosorbents.

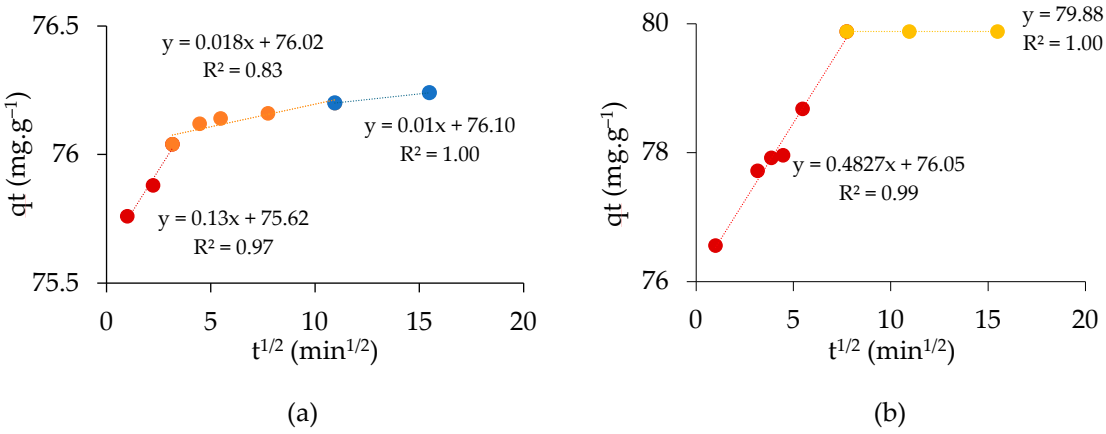

Figure 9. Weber–Morris plots for Zn ions adsorption onto AN (**a**) and AB (**b**), showing three-stage and two-stage diffusion behaviors, respectively.

For both adsorbents, the plots of qt versus $t^{1/2}$ exhibited multilinearity, indicating that Zn(II) adsorption proceeds through multiple consecutive steps rather than being governed by a single rate-limiting mechanism. Moreover, none of the linear segments passed through the origin, confirming that intraparticle diffusion is not the sole controlling step and that external mass transfer (boundary layer diffusion) plays a significant role in the overall adsorption process.

For natural acacia, three distinct linear regions were identified in the intraparticle diffusion model. The first region showed a relatively high intraparticle diffusion rate constant (kid_1 = 0.13 mg $g^{-1}min^{-1/2}$), indicating a rapid initial uptake of Zn ions. The second region exhibited a much lower diffusion rate (kid_2 = 0.018 mg $g^{-1}min^{-1/2}$) along with a

reduced correlation coefficient. In the third region, the diffusion rate further decreased (kid_3 = 0.01 mg $g^{-1}min^{-1/2}$), corresponding to the equilibrium stage.

Charcoal fines only displayed two linear regions, the first one with substantially higher intraparticle diffusion rate constant, showing a very high diffusion rate (kid_1 = 0.48 mg $g^{-1}min^{-1/2}$). In the second stage, the curve became horizontal, indicating equilibrium.

4. Discussion

4.1. Samples Characterization

The morphological analyses provide important insights into the effects of thermal treatment on *Acacia dealbata* biomass and its implications for adsorption performance.

The SEM micrographs (Figures 1 and 2) clearly show that both materials have a heterogeneous and porous structure characterized by cellular structures with different cell types (e.g., rays, vessels and fibers) that are characteristic of hardwoods and of Acacia species [35,36]. The cellular-derived characteristics were retained in the charcoal fines with the pyrolysis process substantially enhancing the surface porosity of the material. The charcoal fines exhibited a rougher and more heterogeneous surface compared with the natural biomass, suggesting a significant increase in the number of accessible adsorption sites. According to the EDS results, the charcoal fines contain higher concentrations of calcium (Ca) and magnesium (Mg), in agreement with the known mineral composition of *A. dealbata* wood, which also presents notable potassium (K) levels (1.77 mg g^{-1}) [37]. A high content in Ca was also observed in sugarcane bagasse biochar [30].

The higher percentages of Ca and Mg in the charcoal fines compared with native *A. dealbata* wood, result from the thermal degradation of organic matter during pyrolysis, which concentrates non-volatile mineral elements in the solid residue and increases their surface detectability in EDS analysis.

The morphological characteristics observed are consistent with those reported for other Acacia species. For instance, *A. nilotica* leaves exhibit a fibrous, amorphous surface rich in oxygenated functional groups capable of interacting with heavy metal ions [23]. Similarly, *Acacia* spp. leaves and their citric acid-modified forms display irregular surfaces dominated by carbon and oxygen elements, as confirmed by EDS analysis [38].

The XRD analysis shows the appearance of calcite ($CaCO_3$) peaks in the charcoal fines, absent in the natural biomass, with its characteristic diffraction reflections explicitly identified at 2θ = 29.4°, 36.0°, 39.4° and 43.1°, indicating mineral transformation during pyrolysis, which can enhance the surface alkalinity and ion-exchange potential. In the AN, the characteristic amorphous cellulose peak was explicitly identified at 2θ ≈ 22°, corresponding to cellulose type I. The diffraction peaks at 2θ = 14.9°, 16.2°, and 22° are characteristic of cellulose type I structures [37,39], while a peak near 25° reflects partial crystallization and improved structural ordering [40]. Similar amorphous cellulose regions have been reported for *Acacia* spp. [38], and for activated carbon derived from *A. mangium*, which presents an amorphous carbon matrix with broad peaks at 26° and 44° [41]. These findings indicate that the carbonization of *A. dealbata* biomass preserves part of the cellulose structure while promoting a transition to a more ordered carbonaceous matrix, favorable for adsorption processes.

The surface area of *A. dealbata* charcoal fines (33 m^2 g^{-1}) was significantly higher than the natural material (1.4 m^2 g^{-1}). These results confirm that thermal treatment effectively increased the surface area. Similarly, chemical activation has been shown to drastically increase surface area in *A. auriculiformis* biosorbent, whose activation with sulfuric acid expanded the surface area from 1.9 to 891.4 m^2 g^{-1} [42].

However, the obtained values of surface areas remain lower than those reported for other biochars of Acacia species, 103.47, 377.18 and 394 $m^2\ g^{-1}$ [41,43,44], although similar to that obtained for cork pyrolyzed at 450 °C, of 31.8 $m^2\ g^{-1}$ [45], and higher than those reported for sugarcane bagasse biochar, 12.63 $m^2\ g^{-1}$ [30]. This pattern suggests that the applied pyrolysis conditions enabled partial pore development without generating the extensive micro/mesoporosity typical of chemically activated materials.

Pores are generally classified as micropores (diameter < 2 nm), mesopores (2–50 nm), and macropores (>50 nm) [46]. In this study, the charcoal fines (AB) exhibited both macroporous and mesoporous structures, with a broader pore width distribution (2–122 nm) compared with natural acacia (AN), which presented predominantly mesoporous characteristics (2–33 nm). In contrast, biochar derived from sugarcane bagasse exhibited a predominantly microporous structure (1.58 nm) [30], whereas biochar from *Eucalyptus* sp. and activated carbon from *A. mangium* presented mesoporous structures, with pore diameters of 2.37 nm and 5.51–11.8 nm, respectively [34,40]. The pore heterogeneity and wider distribution in AB are advantageous for adsorption processes, as they facilitate the retention of a broader range of contaminant molecules with different sizes and diffusion properties.

Regarding pore volume, values were 0.004 $cm^3\ g^{-1}$ and 0.030 $cm^3\ g^{-1}$ for natural acacia (AN) and charcoal fines (AB), respectively. These values are lower than those reported for other Acacia-based materials, such as *A. nilotica* raw biomass (0.064 $cm^3\ g^{-1}$) and its corresponding biochar (0.091 $cm^3\ g^{-1}$) [44]. Similarly, a significant increase in pore volume was observed for *A. auriculiformis* biosorbent after activation, rising from 0.009 $cm^3\ g^{-1}$ to 0.543 $cm^3\ g^{-1}$ [42]. For comparison, biochar produced from *Eucalyptus* sp. exhibited an intermediate pore volume of 0.174 $cm^3\ g^{-1}$ [40].

When compared with other lignocellulosic biochars, Acacia-derived materials generally exhibit moderate surface areas but favorable morphological features. For example, biochars derived from peanut shells, *Bactris gasipaes*, and corn cobs presented much higher specific surface areas (652.8–1224 $m^2\ g^{-1}$) and larger pore sizes (21.11–30.62 μm) [47].

Overall, these findings reinforce the potential of Acacia biomass, whether in its raw or modified form, as sustainable material for environmental remediation applications. Despite the enhanced textural properties of the charcoal fines, the untreated biomass retains sufficient morphological and chemical functionality to sustain effective metal adsorption, representing a low-cost alternative without energy-intensive processing.

4.2. Effect of the pH, Isotherm and Kinetics

In the present study, the maximum removal of Zn ions was achieved at pH near 7, with efficiencies of approximately 95.3% for natural acacia (AN) and 98.4% for acacia charcoal fines (AB). Although higher removal values were recorded at pH above 7, these may be attributed to the precipitation of zinc hydroxide ($Zn(OH)_2$), rather than to adsorption alone. Results presented before show that there is almost no soluble zinc for pH over 7 [48]. At the optimal pH, residual Zn concentrations after treatment were <2 mg L^{-1} for both AN and AB. These values comply with internationally accepted standards for treated water, including the WHO guideline value (3 mg L^{-1}) and the EU Industrial Wastewater Discharge Limit (2–5 mg L^{-1}). This confirms that the adsorption efficiencies observed in Figure 6 correspond to effective reductions in dissolved zinc to levels consistent with regulatory thresholds.

The influence of pH on adsorption performance has been examined across different Acacia species. In the simultaneous removal of Ni and aminoazobenzene (dye) by *A. nilotica* leaves, maximum adsorption efficiencies were achieved at pH 4 (87.6%) for the dye and pH 6 (97.8%) for Ni [25]. Likewise, the highest removal rates were reported at pH 6,

using *A. arabica* sawdust for the removal of Hg (99.4%), Cr(VI) (99.3%), Pb (94.6%), and Cu (92.2%) [49].

However, other studies reported that the optimal pH for Pb and Cd removal occurred at 3 and 5, respectively [23], whereas *A. leucocephala* bark exhibited maximum adsorption for Cu, Cd, and Pb at pH 6, 5, and 4, respectively [50]. In opposition, the highest phosphate removal from aqueous solutions using *A. tortilis* pruning waste was observed at pH 8.5 [43].

The point of zero charge (pHpzc) of *A. dealbata* biomass has been reported to range between 4.73 and 5.29 for leaves and branches [37], suggesting that enhanced cation adsorption occurs at pH above 5.29, where the biosorbent surface becomes negatively charged. Similarly, the pHpzc of modified *A. tortilis* biochar was 5.3, and 6.5 for *A. saligna* leaves, with an optimal pH of 6.7 for methylene blue adsorption [24], and pH 8.5 for phosphate adsorption [43]. The results obtained in the present study are consistent with these findings.

For AN, adsorption equilibrium was reached rapidly, approximately 10 min after the beginning of the reaction. In contrast, AB required a longer time to reach saturation, around 120 min. Additionally, the more mineral-enriched surface of the charcoal fines could lead to competitive interactions between active sites, resulting in less stable adsorption process over time. Comparable equilibrium times have been reported for other Acacia-based biosorbents: 20 min [24,51], 30 min [23,51], and 40 min [25], respectively. In contrast, longer equilibration times were required for *A. leucocephala* bark (180 min) [50], and treated *A. arabica* sawdust (48–72 h) [49].

Regarding the adsorption isotherm, the experimental data for Zn adsorption onto both natural acacia (AN) and acacia charcoal fines (AB) were best fitted by the Freundlich model (R^2 = 0.95 and 0.85, respectively), suggesting a multilayer adsorption process occurring on a heterogeneous surface with active sites of varying adsorption energies. Similarly, the competitive adsorption of Pb, Cu, and Zn ions onto rice straw biochar also followed the Freundlich model, with correlation coefficients ranging from 0.91 to 0.93 [52]. Likewise, Zn adsorption onto bamboo, *Acacia* spp., and rice husk biochars was best described by the same model, showing high correlation coefficients (R^2 = 0.97–0.99), further supporting the multilayer and heterogeneous nature of the adsorption mechanism [53].

In contrast, Pb and Cd adsorption onto *A. nilotica* bark followed the Langmuir model more closely (R^2 = 0.879), while Cd adsorption exhibited poor correlations with both Langmuir (R^2 = 0.09) and Freundlich (R^2 = 0.03) models [23]. For *A. saligna* leaves, the experimental data were best represented by the Langmuir isotherm model (R^2 = 0.993) [24]. For *A. nilotica* leaves, isotherm modeling revealed that Ni adsorption involved both monolayer and multilayer processes, with high correlation coefficients for both Langmuir (R^2 = 0.999) and Freundlich (R^2 = 0.941) models, whereas aminoazobenzene adsorption was predominantly monolayer, following the Langmuir model (R^2 = 0.980) [25]. Similarly, the removal of Cr(VI), Pb, Hg, and Cu by *A. arabica* sawdust was consistent with both Langmuir (R^2 = 0.97–0.99) and Freundlich (R^2 = 0.99–1.00) isotherm models [49].

The maximum adsorption capacities (qmax) estimated by the Langmuir model were comparable for AN and AB, with 23.36 mg g^{-1} and 23.79 mg g^{-1}, respectively. A similar trend was reported for *A. nilotica* activated carbon and its raw precursor, with maximum adsorption capacities of 34.79 and 41.01 mg g^{-1}, respectively [51]. Conversely, the maximum monolayer adsorption capacities for *A. nilotica* leaves were 0.60 mg g^{-1} for Ni and 0.35 mg g^{-1} for aminoazobenzene [25]. For treated *A. arabica* sawdust, the adsorption capacities were 111.61 mg g^{-1} for Cr(VI), 52.38 mg g^{-1} for Pb, 20.62 mg g^{-1} for Hg, and 5.64 mg g^{-1} for Cu, respectively [49].

Table 3 compares the results obtained in this study with previously reported data on Zn ion adsorption, allowing the identification of the most favorable conditions for zinc removal across different environmental settings.

Table 3. Comparison of Zn ions adsorption performance using different adsorbents reported in the literature.

Adsorbent	Concentrations of Zn Tested	Best Adsorbent Dosage (g L^{-1})	Optimized pH	Equilibrium Time (h)	Maximum Capacity (qmax Langmuir)	Reference
Clarified sludge (steel industry)	10–100 mg L^{-1}	10	5.0	1	15.53 mg g^{-1}	[54]
Rice husk ash	10–100 mg L^{-1}	10	5.0	3	14.30 mg g^{-1}	[54]
Activated alumina	10–100 mg L^{-1}	10	5.0	4	13.69 mg g^{-1}	[54]
Azadirachta indica (Neem) bark	10–100 mg L^{-1}	10	5.0	4	13.29 mg g^{-1}	[54]
Pinus pinea pinecones	10–50 mg L^{-1}	4	7.0	0.5	7.92 mg g^{-1}	[55]
Crab shell	0.2–40 mM	1	6.0	-	2.83 mmol g^{-1}	[56]
Lemna gibba	0.2–30 mM	1	6.0	-	0.85 mmol g^{-1}	[57]
Ziziphus joazeiro bark	20.2–443.1 mg L^{-1}	0.4	5.5	1	13.12 mg g^{-1}	[58]
Sargassum ilicifolium	60–300 mg L^{-1}	0.2	6.0	1	2.78 mmol g^{-1}	[59]
Acacia dealbata biomass (AN)	10–50 mg L^{-1}	4	7.0	0.17	23.36 mg g^{-1}	Present study
A. dealbata charcoal fines (AB)	10–50 mg L^{-1}	4	7.0	2	23.79 mg g^{-1}	Present study

Overall, it is observed that most materials exhibit better performance at slightly acidic to neutral pH values (pH 5–7), which is consistent with the chemical behavior of zinc in aqueous solution. Equilibrium times vary considerably among the materials, reflecting differences in the accessibility of active sites. Lignocellulosic materials or biomass generally show variable performances associated with their chemical composition. In this context, *Acacia dealbata* biomass, in both forms, stands out by presenting significantly higher maximum adsorption capacities (≈23 mg g^{-1}), combined with relatively short equilibrium times.

The PFO model showed a relatively poor description of the experimental data for both biosorbents. For AN, a low correlation coefficient (R^2 = 0.78) was obtained, and the calculated equilibrium adsorption capacity (q_e calc = 0.57 mg g^{-1}) was far lower than the experimental value (q_e exp = 76.14 mg·g^{-1}). Although the PFO fit improved for AB (R^2 = 0.95), the calculated adsorption capacity (q_e calc = 1.00 mg g^{-1}) still deviated significantly from the experimental value (q_e exp = 79.88 mg g^{-1}). These discrepancies indicate that the PFO model is inadequate for describing the overall Zn adsorption process, suggesting that the uptake is not governed solely by physical adsorption or external mass-transfer processes.

In contrast, the PSO model provided an excellent fit for the kinetic data of both biosorbents, as evidenced by correlation coefficients of R^2 = 1.00, and a very close agreement

between calculated (q_e calc = 76.24 mg g^{-1} and 80.00 mg g^{-1}, for AN and AB, respectively) and experimental adsorption capacities (q_e exp = 76.14 mg g^{-1} for AN, and 79.88 mg g^{-1} for AB). This strong conformity indicates that the PSO model more accurately represents Zn adsorption onto both materials, implying that chemisorption involving valence forces or electron exchange between Zn(II) ions and surface functional groups is the dominant rate-controlling mechanism.

The PSO kinetic parameters further highlight differences in adsorption behavior between AN and AB. Natural acacia exhibited a significantly higher PSO rate constant (k_2 = 3.85 × 10^{-1} g $mg^{-1}min^{-1}$) and a much higher initial adsorption rate (h = 2240.65 mg $g^{-1}min^{-1}$) compared to charcoal fines (k_2 = 4.16 × 10^{-2} g $mg^{-1}min^{-1}$; h = 266.54 mg $g^{-1}min^{-1}$). These results suggest that Zn uptake occurs more rapidly on AN during the initial stages, likely due to the high accessibility of reactive functional groups such as hydroxyl and carboxyl groups on the surface.

Despite the faster initial kinetics observed for AN, charcoal fines achieved a slightly higher equilibrium adsorption capacity. This behavior may be attributed to the more developed porous structure and higher surface area of AB, which allow Zn ions to gradually diffuse into internal adsorption sites, leading to enhanced uptake at equilibrium. Therefore, while AN favors rapid Zn binding, AB provides a marginally higher ultimate adsorption capacity.

Overall, the kinetic analysis demonstrates that Zn adsorption onto both natural and charcoal fines of acacia is best described by the pseudo-second-order model, with chemisorption playing a dominant role. The contrasting kinetic parameters emphasize that AN is more effective for rapid Zn removal, whereas charcoal fines are advantageous when higher equilibrium adsorption is required. Consistent with these findings, a better fit with the PSO model have been reported for the sorption of Pb, Cu and Zn (R^2 = 0.99) [52], Zn, Cu and Ni (R^2 = 0.95 to 1.00) [59], Ni and aminoazobenzene (R^2 = 0.99) [25], methylene blue (R^2 = 1.00) [24], Cd (R^2 = 0.999) and Pb (R^2 = 0.988) [23], as well as for reactive black 5, with R^2 ranging from 0.972 to 0.998 [51].

Even though PSO model is the most used model to describe adsorption suggesting that chemisorption is the main process, in accordance with Aguila-Rosas et al. [60], it also raises concerns about how researchers often use the PSO model without enough proof. Simply having a good mathematical fit on a graph is not enough to prove how a chemical reaction is controlled. These authors state that to truly confirm the mechanism, it is needed more than just curve-fitting. Supporting data from other tests, such as checking how kinetics change with temperature, calculating the heat of the process (isosteric enthalpy), or using spectroscopy to prove that actual chemical bonds are forming are needed.

A direct comparison of the two materials by the intraparticle diffusion model reveals that while both follow a similar multistep adsorption mechanism, charcoal fines demonstrate faster adsorption kinetics and higher intraparticle diffusion rates at all stages.

For AN, three distinct linear regions were observed. The relatively low diffusion constants across all stages reflect the limited porosity and pore connectivity of natural acacia, has seen in Figure 4, which restrict Zn ions transport into the internal structure. In contrast, AB only exhibited two linear regions with the first one presenting significantly higher intraparticle diffusion rate constant, indicating extremely rapid Zn(II) uptake, reflecting the higher surface area (33 m^2g^{-1}). The equilibrium adsorption capacity calculated by this model was ~80 mg g^{-1} for AB, higher than that of AN (~76 mg g^{-1}).

In summary, no significant differences were observed between the two materials investigated, natural acacia (AN) and acacia charcoal fines (AB), under the conditions evaluated. In both cases, the adsorption process proceeded predominantly through multilayer chemisorption, with comparable maximum adsorption capacities. These results indicate

that both biosorbents exhibit a similar affinity for zinc ions and possess sufficient surface functionality to promote effective metal ion retention. However, when considering the substantial energy requirements associated with the thermal treatment needed to produce charcoal fines, natural acacia stands out as the most cost-effective and sustainable option.

Comparable trends have been reported for other biomass biochar systems. For instance, Ginkgo (*Spiraea blumei*) leaves, peanut (*Arachis hypogaea Linn.*) shells, and *Metasequoia glyptostroboides* leaves were evaluated for Pb and Cu adsorption alongside their corresponding biochars. Among them, only Ginkgo-derived biochar exhibited enhanced adsorption capacity after pyrolysis [61]. This finding reinforces that, although biochar is generally recognized for its effectiveness in heavy metal adsorption, its performance is not always superior to that of the original biomass, as the adsorption efficiency strongly depends on feedstock composition and treatment conditions.

In addition to adsorption performance, practical aspects related to material handling and end-of-life management were considered. After Zn(II) uptake, both AN and AB can be safely managed through stabilization/solidification, incorporation into ceramic or composite matrices, or regeneration using mild acidic eluents, all of which minimize metal leaching and are widely reported as effective disposal routes for metal-loaded biosorbents [62,63]. Regarding the charcoal fines used as AB, the pyrolysis of *A. dealbata* biomass typically yields three product streams—solid biochar, condensable liquids, and non-condensable gases. Because the AB used in this study was supplied as an industrial by-product, only the solid fraction was relevant here; however, the literature reports that condensable liquids are generally rich in water and light organics and can be treated using conventional wastewater processes, whereas non-condensable gases are commonly combusted for energy recovery or thermal oxidation [64]. These considerations support the environmental feasibility of implementing acacia-derived materials in water treatment while ensuring compliant management of both process by-products and metal-enriched residues.

5. Conclusions

From a practical standpoint, the similar adsorption behavior of natural (AN) and carbonized acacia (AB) suggests that the simpler, untreated biomass may serve as an equally efficient and more sustainable alternative for zinc removal from aqueous solutions at least within the studied conditions. Nevertheless, higher surface area and structural porosity achieved in the charcoal fines, could offer advantages in a long-term or continuous treatment applications.

Overall, these findings highlight the potential of Acacia-based biosorbents as low-cost, environmentally friendly materials for wastewater remediation, particularly in regions where acacia species are abundant and often considered invasive. The valorization of invasive biomass also contributes to ecosystem management efforts by providing an added-value pathway for material that would otherwise require costly disposal.

Future studies should focus on regeneration efficiency of the adsorbent material, adsorption in multi-metal systems, and large-scale application under real wastewater conditions. Additional work assessing long-term stability, leaching behavior and safe end-of-life handling of metal-loaded biosorbents will further support their deployment in real treatment systems.

Author Contributions: Conceptualization, M.M.; methodology, M.M., H.P., L.C.-L., L.G., A.P.F.C., R.N. and B.E.; software, M.M., J.S.P., A.P.F.C., R.N. and L.C.-L.; investigation, M.M., J.S.P. and A.P.F.C.; writing—original draft preparation, M.M.; writing—review and editing, M.M., H.P., L.C.-L., B.E., A.P.F.C., R.N. and L.G.; supervision, H.P., L.C.-L., B.E., R.N. and L.G. All authors have read and agreed to the published version of the manuscript.

Funding: This research was funded by national funds through the FCT—Foundation for Science and Technology, I.P., through a doctoral scholarship (reference 2023.03677.BDANA; DOI: 10.54499/2023.03677.BDANA). Additional funding was provided by national funds through the FCT—Foundation for Science and Technology, I.P., within the scope of the CERNAS–IPV Research Centre project UIDB/00681/2025 (DOI: 10.54499/UID/00681/2025), and by the Forest Research Centre (CEF) under projects UID/00239/2025 (DOI: 10.54499/UID/00239/2025) and UID/PRR/00239/2025 (DOI: 10.54499/UID/PRR/00239/2025).

Data Availability Statement: The original contributions presented in this study are included in the article. Further inquiries can be directed to the corresponding authors.

Acknowledgments: The authors would like to thank the Polytechnic Institute of Viseu and the University of Aveiro for their support. This work was developed within the scope of the projects CICECO-Aveiro Institute of Materials, UIDB/50011/2020 (DOI 10.54499/UIDB/50011/2020), UIDP/50011/2020 (DOI 10.54499/UIDP/50011/2020) and LA/P/0006/2020 (DOI 10.54499/LA/P/0006/2020), financed by national funds through the FCT/MCTES (PIDDAC).

Conflicts of Interest: Author Lucas Grosche was employed by the company 4iTec Lusitânia S.A., Lugar do Pombal, Zona Industrial do Salgueiro. The remaining authors declare that the research was conducted in the absence of any commercial or financial relationships that could be construed as a potential conflict of interest.

References

1. Lorenzo, P.; González, L.; Reigosa, M.J. The Genus Acacia as Invader: The Characteristic Case of *Acacia dealbata* Link in Europe. *Ann. For. Sci.* **2010**, *67*, 101. [CrossRef]
2. Lazzaro, L.; Giuliani, C.; Fabiani, A.; Agnelli, A.E.; Pastorelli, R.; Lagomarsino, A.; Benesperi, R.; Calamassi, R.; Foggi, B. Soil and Plant Changing after Invasion: The Case of *Acacia dealbata* in a Mediterranean Ecosystem. *Sci. Total Environ.* **2014**, *497–498*, 491–498. [CrossRef] [PubMed]
3. Nunes, L.J.R.; Raposo, M.A.M.; Meireles, C.I.R.; Pinto Gomes, C.J.; Ribeiro, N.M.C.A. Control of Invasive Forest Species through the Creation of a Value Chain: *Acacia dealbata* Biomass Recovery. *Environments* **2020**, *7*, 39. [CrossRef]
4. Raposo, M.A.M.; Pinto Gomes, C.J.; Nunes, L.J.R. Evaluation of Species Invasiveness: A Case Study with *Acacia dealbata* Link. on the Slopes of Cabeça (Seia-Portugal). *Sustainability* **2021**, *13*, 11233. [CrossRef]
5. Nunes, L.J.R.; Meireles, C.I.R.; Pinto Gomes, C.J.; Almeida Ribeiro, N.M.C. Historical Development of the Portuguese Forest: The Introduction of Invasive Species. *Forests* **2019**, *10*, 974. [CrossRef]
6. Morais, M.; Marchante, E.; Marchante, H. Big Troubles Are Already Here: Risk Assessment Protocol Shows High Risk of Many Alien Plants Present in Portugal. *J. Nat. Conserv.* **2017**, *35*, 1–12. [CrossRef]
7. ICNF. *6º Inventário Florestal Nacional—Relatório Final*; Instituto da Conservação da Natureza e das Florestas: Lisboa, Portugal, 2019.
8. Bowd, E.J.; Blair, D.P.; Lindenmayer, D.B. Prior Disturbance Legacy Effects on Plant Recovery Post-High-Severity Wildfire. *Ecosphere* **2021**, *12*, e03480. [CrossRef]
9. Jesus, J.G.d.; Tenreiro, R.; Máguas, C.; Trindade, H. *Acacia longifolia*: A Host of Many Guests Even after Fire. *Diversity* **2020**, *12*, 250. [CrossRef]
10. Pereira, M.G.; Gonçalves, N.; Amraoui, M. The Influence of Wildfire Climate on Wildfire Incidence: The Case of Portugal. *Fire* **2024**, *7*, 234. [CrossRef]
11. Gordon, C.E.; Price, O.F.; Tasker, E.M.; Denham, A.J. *Acacia* Shrubs Respond Positively to High Severity Wildfire: Implications for Conservation and Fuel Hazard Management. *Sci. Total Environ.* **2017**, *575*, 858–868. [CrossRef]
12. Pieterse, P.J.; Boucher, C. Is Burning a Standing Population of Invasive Legumes a Viable Control Method? Effects of a Wildfire on an Acacia Mearnsii Population. *S. Afr. For. J.* **1997**, *180*, 15–21. [CrossRef]
13. Riveiro, S.F.; Cruz, Ó.; Casal, M.; Reyes, O. Fire and Seed Maturity Drive the Viability, Dormancy, and Germination of Two Invasive Species: *Acacia longifolia* (Andrews) Willd. and Acacia Mearnsii De Wild. *Ann. For. Sci.* **2020**, *77*, 60. [CrossRef]
14. Marchante, H.; Freitas, H.; Hoffmann, J.H. Seed Ecology of an Invasive Alien Species, *Acacia longifolia* (Fabaceae), in Portuguese Dune Ecosystems. *Am. J. Bot.* **2010**, *97*, 1780–1790. [CrossRef] [PubMed]
15. Presidência do Conselho de Ministros. *Decreto-Lei n.º 92/2019: Regime Jurídico Aplicável Ao Controlo, à Detenção, à Introdução Na Natureza e Ao Repovoamento de Espécies Exóticas Da Flora e Da Fauna*; Imprensa Nacional Casa da Moeda: Lisboa, Portugal, 2019; pp. 3428–3442.

16. Le Maitre, D.C.; Gaertner, M.; Marchante, E.; Ens, E.-J.; Holmes, P.M.; Pauchard, A.; O'Farrell, P.J.; Rogers, A.M.; Blanchard, R.; Blignaut, J.; et al. Impacts of Invasive Australian Acacias: Implications for Management and Restoration. *Divers. Distrib.* **2011**, *17*, 1015–1029. [CrossRef]
17. Correia, R.; Quintela, J.C.; Duarte, M.P.; Gonçalves, M. Insights for the Valorization of Biomass from Portuguese Invasive *Acacia* spp. in a Biorefinery Perspective. *Forests* **2020**, *11*, 1342. [CrossRef]
18. Correia, R.; Duarte, M.P.; Maurício, E.M.; Brinco, J.; Quintela, J.C.; da Silva, M.G.; Gonçalves, M. Chemical and Functional Characterization of Extracts from Leaves and Twigs of *Acacia dealbata*. *Processes* **2022**, *10*, 2429. [CrossRef]
19. Oliveira, C.S.D.; Moreira, P.; Resende, J.; Cruz, M.T.; Pereira, C.M.F.; Silva, A.M.S.; Santos, S.A.O.; Silvestre, A.J.D. Characterization and Cytotoxicity Assessment of the Lipophilic Fractions of Different Morphological Parts of *Acacia dealbata*. *Int. J. Mol. Sci.* **2020**, *21*, 1814. [CrossRef]
20. Resende, M.D.V.; Rezende, G.D.S.P.; Demuner, B. *Utilização de Espécies Do Gênero Acacia Na Produção de Celulose de Fibra Curta No Sudeste Asiático e Na África*; Embrapa Florestas: Curitiba, Brazil, 2001; pp. 15–39.
21. Yáñez, R.; Romaní, A.; Garrote, G.; Alonso, J.L.; Parajó, J.C. Experimental Evaluation of Alkaline Treatment as a Method for Enhancing the Enzymatic Digestibility of Autohydrolysed *Acacia dealbata*. *J. Chem. Technol. Biotechnol.* **2009**, *84*, 1070–1077. [CrossRef]
22. Lourenço, A.; Baptista, I.; Gominho, J.; Pereira, H. The Influence of Heartwood on the Pulping Properties of Acacia Melanoxylon Wood. *J. Wood Sci.* **2008**, *54*, 464–469. [CrossRef]
23. Adam, A.B.; Hyelalibia, A.; Akinterinwa, A. Modification and Characterazation of Acacia Nilotica Leaves and Its Application in Water Treatment. *Chem. Res. Technol.* **2024**, *1*, 192–203. [CrossRef]
24. Terkhi, M.C.; Belhaine, A.; Abdelmalek, F.; Ghezzar, M.R.; Addou, A. *Acacia saligna* Leaves: A Potential New Low-Cost Adsorbent for Removal of Methylene Blue from Aqueous Solutions. *Desalination Water Treat.* **2023**, *300*, 178–191. [CrossRef]
25. Murtaza, G.; Ditta, A.; Ahmed, Z.; Usman, M.; Faheem, M.; Tariq, A. Co-Biosorption Potential of Acacia Nilotica Bark in Removing Ni and Aminoazobenzene from Contaminated Wastewater. *Desalination Water Treat.* **2021**, *233*, 261–270. [CrossRef]
26. López-Hortas, L.; Rodríguez-González, I.; Díaz-Reinoso, B.; Torres, M.D.; Moure, A.; Domínguez, H. Tools for a Multiproduct Biorefinery of *Acacia dealbata* Biomass. *Ind. Crops Prod.* **2021**, *169*, 113655. [CrossRef]
27. Ferreira, S.; Gil, N.; Queiroz, J.A.; Duarte, A.P.; Domingues, F.C. An Evaluation of the Potential of *Acacia dealbata* as Raw Material for Bioethanol Production. *Bioresour. Technol.* **2011**, *102*, 4766–4773. [CrossRef]
28. Plum, L.M.; Rink, L.; Haase, H. The Essential Toxin: Impact of Zinc on Human Health. *Int. J. Environ. Res. Public Health* **2010**, *7*, 1342–1365. [CrossRef]
29. Pérez-Marín, A.B.; Ortuño, J.F.; Aguilar, M.I.; Lloréns, M.; Meseguer, V.F. Competitive Effect of Zinc and Cadmium on the Biosorption of Chromium by Orange Waste. *Processes* **2024**, *12*, 148. [CrossRef]
30. Poonam; Bharti, S.K.; Kumar, N. Kinetic Study of Lead (Pb^{2+}) Removal from Battery Manufacturing Wastewater Using Bagasse Biochar as Biosorbent. *Appl. Water Sci.* **2018**, *8*, 119. [CrossRef]
31. Park, J.-H.; Ok, Y.S.; Kim, S.-H.; Cho, J.-S.; Heo, J.-S.; Delaune, R.D.; Seo, D.-C. Competitive Adsorption of Heavy Metals onto Sesame Straw Biochar in Aqueous Solutions. *Chemosphere* **2016**, *142*, 77–83. [CrossRef]
32. Weber, W.J.; Morris, J.C. Kinetics of Adsorption on Carbon from Solution. *J. Sanit. Engrg. Div.* **1963**, *89*, 31–59. [CrossRef]
33. Thommes, M.; Kaneko, K.; Neimark, A.V.; Olivier, J.P.; Rodriguez-Reinoso, F.; Rouquerol, J.; Sing, K.S.W. Physisorption of Gases, with Special Reference to the Evaluation of Surface Area and Pore Size Distribution (IUPAC Technical Report). *Pure Appl. Chem.* **2015**, *87*, 1051–1069. [CrossRef]
34. Danish, M.; Hashim, R.; Ibrahim, M.N.M.; Rafatullah, M.; Ahmad, T.; Sulaiman, O. Characterization of Acacia Mangium Wood Based Activated Carbons Prepared in the Presence of Basic Activating Agents. *BioRessourses* **2011**, *6*, 3019–3033. [CrossRef]
35. Whinder, F.; Clarke, K.L.; Warwick, N.W.M.; Gasson, P.E. Structural Diversity of the Wood of Temperate Species of Acacia s.s. (Leguminosae: Mimosoideae). *Aust. J. Bot.* **2013**, *61*, 291–301. [CrossRef]
36. Tavares, F.; Quilhó, T.; Pereira, H. Wood and Bark Fiber Characteristics of Acacia Melanoxylon and Comparison to Eucalyptus Globules. *CERNE* **2011**, *17*, 61–68. [CrossRef]
37. Macena, M.; Cruz-Lopes, L.; Grosche, L.; Santos-Vieira, I.; Esteves, B.; Pereira, H. Characterization of Lignocellulosic Byproducts from the Portuguese Forest: Valorization and Sustainable Use. *Materials* **2025**, *18*, 4716. [CrossRef] [PubMed]
38. Essekri, A.; Laabd, M.; Fatni, A.; Ait Addi, A.; Lakhmiri, R.; Albourine, A. The Use of Raw and Modified Acacia Leaves for Adsorptive Removal of Crystal Violet from Water. *Chem. Eng. Res. Des.* **2023**, *190*, 143–156. [CrossRef]
39. de Farias, D.T.; Labidi, J.; Pedrazzi, C.; Gatto, D.A.; de Cademartori, P.H.G.; Welter, C.A.; da Silva, G.T.; de Almeida, T.M. Acid-Hydrolysis-Assisted Cellulose Nanocrystal Isolation from Acacia Mearnsii de Wild. *Wood Kraft Pulp. Polymers* **2024**, *16*, 3371. [CrossRef]
40. Dias, J.; Conceição, A.; Delatorre, F.M.; Siqueira, P. Production, Characterization Physical, Chemical, and Structural Analysis of Biochar Fines for Bio-Reinforcement in Composite Materials. *Processes* **2025**, *13*, 504. [CrossRef]

41. Danish, M.; Hashim, R.; Ibrahim, M.N.M.; Rafatullah, M.; Sulaiman, O. Surface Characterization and Comparative Adsorption Properties of Cr(VI) on Pyrolysed Adsorbents of *Acacia Mangium* Wood and *Phoenix Dactylifera* L. Stone Carbon. *J. Anal. Appl. Pyrolysis* **2012**, *97*, 19–28. [CrossRef]
42. Shahnaz, T.; Patra, C.; Sharma, V.; Selvaraju, N. A Comparative Study of Raw, Acid-Modified and EDTA-Complexed Acacia Auriculiformis Biomass for the Removal of Hexavalent Chromium. *Chem. Ecol.* **2020**, *36*, 360–381. [CrossRef]
43. Manawi, Y.; Al-Gaashani, R.; Simson, S.; Tong, Y.; Lawler, J.; Kochkodan, V. Adsorptive Removal of Phosphate from Water with Biochar from Acacia Tree Modified with Iron and Magnesium Oxides. *Sci. Rep.* **2024**, *14*, 17414. [CrossRef]
44. Singh, S.; Prajapati, A.K.; Chakraborty, J.P.; Mondal, M.K. Adsorption Potential of Biochar Obtained from Pyrolysis of Raw and Torrefied Acacia Nilotica towards Removal of Methylene Blue Dye from Synthetic Wastewater. *Biomass Conv. Bioref.* **2023**, *13*, 6083–6104. [CrossRef]
45. Wang, Q.; Lai, Z.; Mu, J.; Chu, D.; Zang, X. Converting Industrial Waste Cork to Biochar as Cu (II) Adsorbent via Slow Pyrolysis. *Waste Manag.* **2020**, *105*, 102–109. [CrossRef] [PubMed]
46. Burwell, R. Manual of Symbolsand Terminology for Physicochemical Quantities and Units-Appendix II. *Pure Appl. Chem.* **1976**, *46*, 71–90. [CrossRef]
47. Puglla, E.P.; Guaya, D.; Tituana, C.; Osorio, F.; García-Ruiz, M.J. Biochar from Agricultural By-Products for the Removal of Lead and Cadmium from Drinking Water. *Water* **2020**, *12*, 2933. [CrossRef]
48. Fischer, A.; Sgolik, L.; Kreller, A.; Dornack, C. Zinc(II) Adsorption by Low-Carbon Shungite: The Effect of pH. *Water* **2018**, *10*, 422. [CrossRef]
49. Meena, A.K.; Kadirvelu, K.; Mishra, G.K.; Rajagopal, C.; Nagar, P.N. Adsorptive Removal of Heavy Metals from Aqueous Solution by Treated Sawdust (*Acacia arabica*). *J. Hazard. Mater.* **2008**, *150*, 604–611. [CrossRef]
50. Munagapati, V.S.; Yarramuthi, V.; Nadavala, S.K.; Alla, S.R.; Abburi, K. Biosorption of Cu(II), Cd(II) and Pb(II) by *Acacia leucocephala* Bark Powder: Kinetics, Equilibrium and Thermodynamics. *Chem. Eng. J.* **2010**, *157*, 357–365. [CrossRef]
51. Amin, M.T.; Alazba, A.A. Comparative Study of the Absorptive Potential of Raw and Activated Carbon Acacia Nilotica for Reactive Black 5 Dye. *Environ. Earth Sci.* **2017**, *76*, 581. [CrossRef]
52. Wang, Y.-Y.; Liu, Y.-X.; Lu, H.-H.; Yang, R.-Q.; Yang, S.-M. Competitive Adsorption of Pb(II), Cu(II), and Zn(II) Ions onto Hydroxyapatite-Biochar Nanocomposite in Aqueous Solutions. *J. Solid State Chem.* **2018**, *261*, 53–61. [CrossRef]
53. Van Hien, N.; Valsami-Jones, E.; Vinh, N.C.; Phu, T.T.; Tam, N.T.T.; Lynch, I. Effectiveness of Different Biochar in Aqueous Zinc Removal: Correlation with Physicochemical Characteristics. *Bioresour. Technol. Rep.* **2020**, *11*, 100466. [CrossRef]
54. Bhattacharya, A.K.; Mandal, S.N.; Das, S.K. Adsorption of Zn(II) from Aqueous Solution by Using Different Adsorbents. *Chem. Eng. J.* **2006**, *123*, 43–51. [CrossRef]
55. Macena, M.; Cruz-Lopes, L.; Grosche, L.; Esteves, B.; Santos-Vieira, I.; Pereira, H. Valorization of Pinecones as Biosorbents for Environmental Remediation of Zn-Contaminated Wastewaters. *Environments* **2025**, *12*, 284. [CrossRef]
56. Morales-Barrera, L.; Cristiani-Urbina, E. Equilibrium Biosorption of Zn2+ and Ni2+ Ions from Monometallic and Bimetallic Solutions by Crab Shell Biomass. *Processes* **2022**, *10*, 886. [CrossRef]
57. Morales-Barrera, L.; Flores-Ortiz, C.M.; Cristiani-Urbina, E. Single and Binary Equilibrium Studies for Ni2+ and Zn2+ Biosorption onto Lemna Gibba from Aqueous Solutions. *Processes* **2020**, *8*, 1089. [CrossRef]
58. Santos, Y.T.d.C.; Costa, G.P.d.; Marcell Coelho Menezes, J.; Victor Serra Nunes, J.; Hosseini-Bandegharaei, A.; Douglas Melo Coutinho, H.; Sena Júnior, D.; José de Paula Filho, F.; Nonato Pereira Teixeira, R. Adsorption of Zn(II) IONS by *Ziziphus Joazeiro* Barks in Aqueous Solutions. *Results Chem.* **2024**, *7*, 101339. [CrossRef]
59. Tabaraki, R.; Nateghi, A. Multimetal Biosorption Modeling of Zn2+, Cu2+ and Ni2+ by *Sargassum Ilicifolium*. *Ecol. Eng.* **2014**, *71*, 197–205. [CrossRef]
60. Aguila-Rosas, J.; Cano, F.J.; Nagaya, A.; Quirino-Barreda, C.T.; Ortiz, M.d.J.M.; Vargas, A.G.; Ibarra, I.A.; Lima, E. MOF-Composites for Adsorption and Degradation of Contaminants in Wastewater. *Chem. Commun.* **2025**, *61*, 11706–11731. [CrossRef] [PubMed]
61. Lee, M.-E.; Park, J.H.; Chung, J.W. Comparison of the Lead and Copper Adsorption Capacities of Plant Source Materials and Their Biochars. *J. Environ. Manag.* **2019**, *236*, 118–124. [CrossRef] [PubMed]
62. Babel, S.; Kurniawan, T.A. Low-Cost Adsorbents for Heavy Metals Uptake from Contaminated Water: A Review. *J. Hazard. Mater.* **2003**, *97*, 219–243. [CrossRef] [PubMed]
63. Simón, D.; Quaranta, N.; Medici, S.; Costas, A.; Cristóbal, A. Immobilization of Zn (II) Ions from Contaminated Biomass Using Ceramic Matrices. *J. Hazard. Mater.* **2019**, *373*, 687–697. [CrossRef]
64. Bridgwater, A.V. Review of Fast Pyrolysis of Biomass and Product Upgrading. *Biomass Bioenergy* **2012**, *38*, 68–94. [CrossRef]